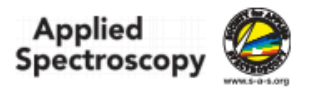


Spectroscopic Techniques



Applied Spectroscopy
2021, Vol. 75(2) 208-215
© The Author(s) 2020
Article reuse guidelines:
sagepub.com/journals-permissions
DOI: 10.1177/0003702820946739
journals.sagepub.com/home/asp

\$SAGE

Suppressing the Multiplex Disadvantage in Photon-Noise Limited Interferometry Using Cross-Dispersed Spatial Heterodyne Spectrometry

Miles J. Egan , Arelis M. Colón, S. Michael Angel , and Shiv K. Sharma

Abstract

Spatial heterodyne spectrometers are members of the static Fourier transform class of spectrometers, well-regarded for their ability to acquire high-resolution, high wavelength precision emission spectra in compact, light footprint packages. In a spatial heterodyne spectrometer experiment, a Fizeau fringe is generated for every spectral feature in a given spectrum, and spatial heterodyne spectrometer records the superposition of all Fizeau fringes in the spectrum on a detector. Hence, the sensitivity of spatial heterodyne spectrometers is constrained by uncorrelated, multiplicative photon noise that limits the detection of spectral features to those that are more luminous than the square root of the total incident flux onto the detector. In essence, powerful spectral features create a rising floor of noise that wash out less luminous features. In the present work, we introduce a novel spectrometer coupling, that being an Amici prism spectrometer in series with spatial heterodyne spectrometer, that correlates photon shot noise along one axis of a detector that in turn suppresses multiplicative photon noise within each row of the interferogram image. We demonstrate that this spectrometer pairing facilitates the measurement of weak Raman spectral features that, in a traditional spatial heterodyne spectrometer measurement, would be washed out by multiplicative photon noise.

Keywords

Spatial heterodyne spectrometer, Raman spectroscopy, multiplex disadvantage, interferometry, photon-noise, multiplex gain

Date received: 19 May 2020; accepted: 29 June 2020

Introduction

Spatial heterodyne spectrometers (SHS) are amplitudemodulating interferometers, capable of producing wavenumber-dependent Fizeau fringes that can be imaged onto a charge-coupled device (CCD). The principle benefit of SHS is that its acceptance angle is greater than dispersive spectrometers of similar dimension because spectral resolution is defined by the minimum change in wavelength that causes a change of half a fringe period across the CCD. For dispersive spectrometers, spectral resolution is proportional to slit width over focal length.2 One can attempt to increase the throughput transmitted through a fixed slit width by increasing the acceptance angle, but this causes aberrations to occur in the spectral reconstruction that causes a diminution in spectral resolution. The larger acceptance angle of SHS is useful in many practical applications, including measuring spectra with large laser spot sizes

or field instruments that experience wide temperature variations where aligning laser spots onto the field-of-view (FOV) of a dispersive spectrometer is challenging at remote-sensing distances. However, SHS' throughput advantage does not typically result in increased sensitivity. When an SHS interferogram is limited by photon noise (e.g., in the ultraviolet-visible, or UV-Vis domain), SHS suffers from the multiplex disadvantage, meaning that photon noise associated with any one spectral feature is distributed multiplicatively into every other spectral bin as well. In effect, a multiplex noise floor, known as the grass, is

Hawaii Institute of Geophysics and Planetology, University of Hawaii at Manoa, Honolulu, HI, USA

Corresponding Author:

Miles J. Egan, University of Hawaii at Manoa, 1680 East-West Road, POST #602, Honolulu, HI 96822, USA.
Email: eganm@hawaii.edu

generated that is proportional to the square root of the total incident flux in the interferogram. As the total incident flux increases, so does the multiplex noise floor, thus limiting the detection of weak spectral features.

When Connes invented the predecessor to SHS, known as SISAM, Jacquinot noted that such an instrument could still be useful in the photon-noise limited domain when spectral density is low (e.g., Raman spectroscopy).3-8 The key to attaining SHS spectra with high signal-to-noise ratios (SNR) is to limit the total incident flux present in the interferogram relative to the desired spectral feature as much as possible. Typically, this is achieved by utilizing bandpass filters that reject spectral light beyond the Nyquist wavelength or that select for desired spectral features. 9.10 This design choice, although effective in limiting multiplicative photon noise, undermines the throughput advantage and wavelength coverage of SHS. Other attempts have been made to limit the spectral density within an SHS interferogram, notably the echelle grating SHS variant that utilizes various high diffraction grating orders to spatially offset narrow bandpasses onto an CCD.11 The echelle grating SHS variant has been demonstrated in a proof-of-concept sense, although wavelength calibration must be performed separately for each diffraction order and cross-interference from different orders makes interpreting echelle SHS spec-

In the past decade or so, a new class of hybrid dispersive-interferometric spectrometers, sometimes referred to as dispersed Fourier transform spectrometers (dFTS), has come to fruition. ^{12–15} In practice, this class of instruments typically find use in replacing cumbersome cross-dispersed echelle spectrometers in experiments where large resolving powers and high wavelength precision are required. Recently, a few authors interested in isotopic quantification via laser-induced breakdown and laser ablation molecular emission spectroscopies have developed novel spectrometers that pair a dispersive element (i.e., prism or grating) in series with a Fabry–Perot etalon. ^{16,17} This combination achieves ultra-high resolution (on the order of 10 pm) and wider wavelength coverages than stand-alone Fabry–Perot etalons by spatially offsetting degenerate harmonics in Airy's function on a CCD.

In the present work, we describe the creation of a new interferometer variant, named the cross-dispersed spatial heterodyne spectrometer (xSHS), that pairs an Amici prism spectrometer in series with an SHS. The benefits of xSHS are manyfold. First, the multiplex disadvantage is severely diminished by limiting the spectral density present in a given row of the CCD to a narrow wavelength coverage. Second, wavenumber-dependent Fizeau fringes attain higher fringe visibility and wider fringe envelopes when compared to traditional SHS measurements as a result of the wavelength coverage represented in a given row being constrained. Third, spectral features beyond the Nyquist limit do not contribute noise as a consequence of cross-dispersion,

thus eliminating the need for bandpass filtering. Fourth, the degeneracy of Fizeau fringes is broken by cross-dispersion, facilitating unambiguous sampling of spatial fringes equidistance from the Littrow wavelength and aliased fringes beyond the Nyquist limit. Fifth, the Amici prism spectrometer provides a low-resolution spectrum covering hundreds of nanometers, which in turn allows an experimentalist to tune the grating angles of SHS to a spectral region of interest with foreknowledge that spectral density is present there. The first proof-of-concept demonstration of this Amici prism and SHS coupling is presented herein.

Theory of Multiplicative Gain

The formulation of SHS figures of merit has been explained in detail elsewhere, and will not be reiterated here. ^{1,10,18} Instead, attention will be focused on UV–Vis interferometers and multiplicative noise. Multiplex gain is defined as the ratio of SNR_{FTS}/SNR_{dispersive} under the limiting assumption that the throughput of the FTS and dispersive instruments under comparison are equal. Kahn¹⁹ was the first to give a mathematical treatment for single-channel, photonnoise limited interferometers, stating that such instruments experience a multiplex gain relative to scanning spectrometers when the signal intensity for a spectral feature of interest is twice the mean intensity of the wavelengths covered by the free spectral range of the interferometer. Later authors, namely Hirschfeld, ²⁰ Luc and Gerstenkorn, ²¹⁻²² Everall and Howard, ²³ and Zhao and McCreery ²⁴ formulated the multiplex gain as follows

$$G_{SNR} = \left[I(\sigma)/N\overline{I(\sigma)}\right]^{1/2}$$
 (1)

where $I(\sigma)$ is the intensity of a single spectral feature, $\overline{I(\sigma)}$ is the mean intensity of the whole spectrum and N is the number of resolution elements. When a single spectral feature is present in the spectrum, G_{SNR} equals one and FTS attains the same SNR as a dispersive grating spectrometer. However, as the number of spectral features increases, the multiplex gain factor, dynamic range of the detector, and SNR of all spectral features decrease simultaneously for multiplexed instruments in the photon noise domain. Therefore, the only way to increase the sensitivity of SHS in this domain is to manipulate the multiplex gain factor in such a way as to minimize $\overline{I(\sigma)}$ relative to $I(\sigma)$. In the following sections, we demonstrate how this can be accomplished using xSHS.

Instrument Design

The xSHS is an Amici prism spectrometer coupled to an SHS (see Fig. 1). Spectral light is collected by a 50 mm focal length Nikon lens and collimated by a 2.54 cm (1-in.), f/2 achromatic lens. The spot size of the collimated beam is

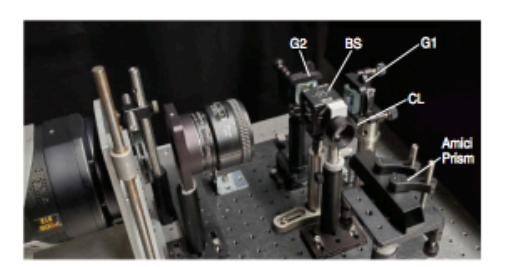


Figure 1. An image of xSHS used in the present work. Collimated light enters the Amici prism. Spectral light is refracted, then focused onto the gratings within SHS by a cylindrical lens. SHS generates Fizeau fringes, which are imaged by a lens and recorded by a CCD.

8 mm in diameter. The spot size of the beam was chosen so that the entirety of the spot could transmit through a commercial, off-the-shelf double Amici prism (hereafter referred to simply as the Amici prism) that possessed a 10 mm entrance window. After transmitting and refracting through the Amici prism, spectral light was focused onto the stationary gratings of SHS by a 75 mm focal length, achromatic cylindrical lens. The transmission efficiency of the Amici prism was 0.78 at 532 nm. The Fizeau fringes produced at the gratings surface were imaged by an 85 mm, f/4 Nikon lens onto a Princeton Instruments PIXIS II CCD. The PIXIS CCD had 2048 pixels along the x-axis and 512 pixels along the y-axis. Each pixel was 13.5 by 13.5 microns. The detector was cooled to -70 °C and so thermal signal was essentially zero (i.e., 0.001 electrons per pixel per second). The resolution of xSHS is governed by the number of lines on the gratings illuminated and the pixel width of the detector. The grating groove density was 150 lines per mm. The maximum measured resolving power was 2116. The linear dispersion provided by the Amici prism on the CCD was approximately 37.7 nm per mm, and the magnification of the gratings onto the CCD was 0.90. Two light sources were used to collect spectra during this experiment. First, an Hg calibration lamp manufactured by Ocean Optics (now Ocean Insight). Second, Raman spectra excited by a 532 nm continuous wave neodymium-doped yttrium aluminum garnet (Nd:YAG) laser, operating at 115 mW. For the Hg measurements, a Semrock FF01-571/572 bandpass filter was used where indicated, and for the Raman measurements, a Semrock E grade edge filter was used to attenuate Rayleigh scattered radiation.

First Light

An Hg calibration lamp provided the spectral light for the first interferogram measured by xSHS. The purpose of the experiment was to show that the 546 nm Hg singlet could be spatially resolved by cross-dispersion from the 577 and

579 nm Hg doublet. The xSHS interferogram of the Hg lamp was collected twice, once with a Semrock FF01-571/ 572 bandpass filter and once without any bandpass filtering whatsoever. If the cross-dispersion was successful, no degradation in the fringe contrast should be observed whether filters were used or not. In addition, the envelope of the interferogram should be broader than a typical SHS interferogram as the breadth of an interferogram envelope is reciprocally dependent upon the wavelength coverage used to generate the interferogram. The raw, unprocessed xSHS interferogram images are presented in Fig. 2. Alongside the xSHS interferograms are SHS interferograms of Hg emission lines where the SHS instrument design is identical in every way to the instrument shown in Fig. I except that the Amici prism and cylindrical lens were removed.

Clearly, the fringe contrast present in the xSHS interferograms is higher than its SHS counterparts. Three Hg lines (i.e., 546.075, 576.961, and 579.067 nm) are present within the wavelength coverage of the bandpass filter. In the xSHS interferograms, two distinct interferogram groupings are resolved. The first, brightest interferogram, located near the top of the image, represents the 546 nm spectral line, while the fainter interferogram directly beneath it is generated by the 577 and 579 nm Hg doublet. For xSHS, the presence of, or lack thereof, bandpass filters played no role in the fringe visibility. This claim is quantified by the fringe visibility numbers quoted in Fig. 3. For SHS, the lack of bandpass filtering increased the background from aliased spectral features, which in turn diminished the fringe visibility dramatically. It is important to emphasize at this point that xSHS attains these higher fringe visibilities while losing \sim 22% of light due to reflections at surfaces of the Amici prism by focusing the remaining light along the y-axis of the grating by the cylindrical lens. In the future, we intend to fabricate custom compound prisms with anti-reflection coatings so that even greater fringe visibilities can be achieved.

Raman xSHS Interferograms

In addition to Hg spectra, several Raman xSHS interferograms were acquired, namely cyclohexane, acetone, acetonitrile, and methanol. For demonstration purposes, we have elected to focus our attention on the acquisition, processing, and noise analysis of cyclohexane's xSHS interferogram alone. The first unprocessed Raman xSHS interferogram of cyclohexane is presented in Fig. 4. The Littrow wavelength was ~532 nm, although the exact wavelength was not known at the time the interferogram was acquired because the grating angles were tuned by manual micrometer screws. The integration time was 10 s. The Raman shift increases as one scans the image from bottom to top. The brightest band, at the top of the image, was contributed by cyclohexane's C–H stretches occurring between

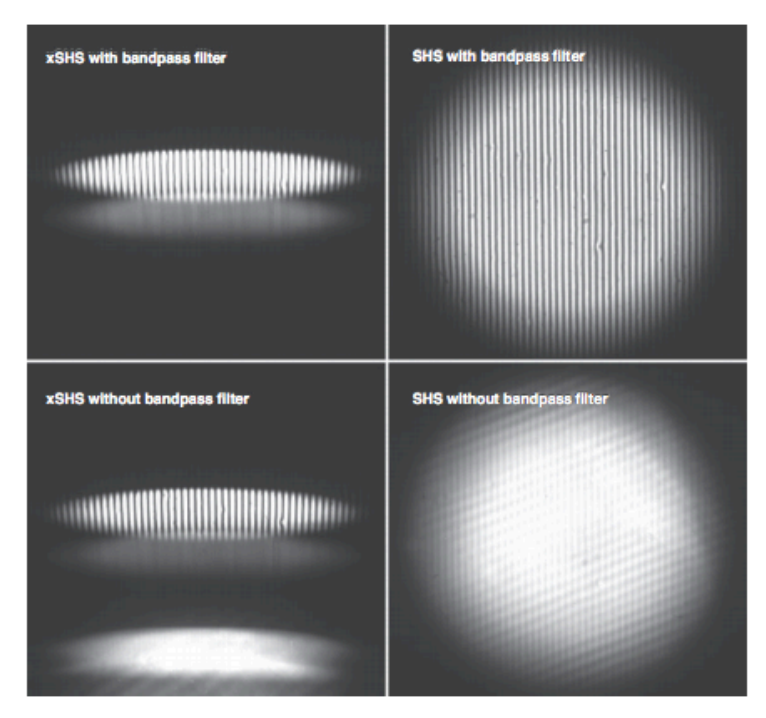


Figure 2. The interferograms of an Hg calibration lamp as measured by xSHS and SHS with and without bandpass filters. Note that the fringe contrast appears brighter for xSHS, even though ~22% of incident light is lost due to reflections at the Amici prism surfaces, as a result of spectral light being focused along the y-axis by a cylindrical lens.

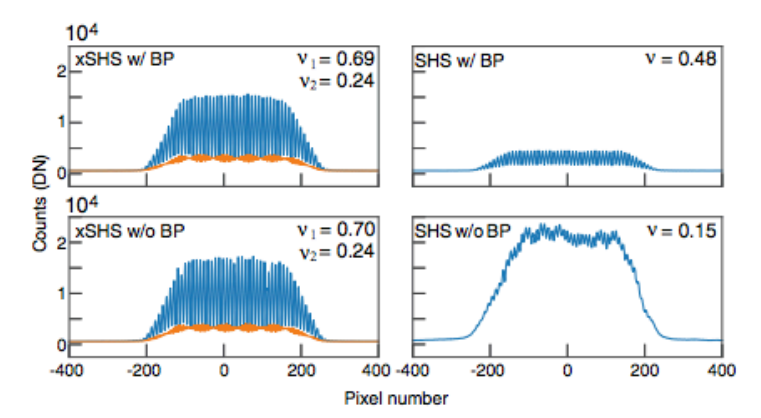


Figure 3. Fringe visibilities were calculated for each interferogram presented in Fig. 2 by taking the brightest row and applying the standard formula $v = I_{max} - I_{min}/I_{max} + I_{min}$. For the xSHS interferograms, v_1 represents the 546 nm fringe (in blue), and v_2 represents the 577 and 579 nm fringes (in orange). Note that no change in the fringe visibility occurs for xSHS when bandpass (BP) filters are removed, while a significant degradation in fringe contrast does occur for SHS.

2800 and 3000 cm-1. Those C-H stretching modes lie contrast near the center of the image is cyclohexane's beyond the Nyquist limit for the defined Littrow angle 801.3 cm-1 Raman mode. Raman modes spaced more xSHS, as will be shown later. The fringe with the highest the CCD by cross-dispersion.

and pixel width, yet were still sampled unambiguously by than ~350 cm⁻¹ apart are completely resolved spatially on

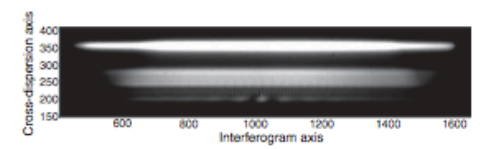


Figure 4. The xSHS interferogram of cyclohexane's Raman spectrum. The Littrow wavelength was \sim 532 nm. As one scans from the bottom of the image to the top, the Raman shift increases. The brightest band at the top of the image is cyclohexane's C–H stretching region. The fringe with the highest contrast at the center of the image is cyclohexane's 801.3 cm $^{-1}$ Raman mode. The xSHS interferogram was windowed to those pixels where spectral light occurred.

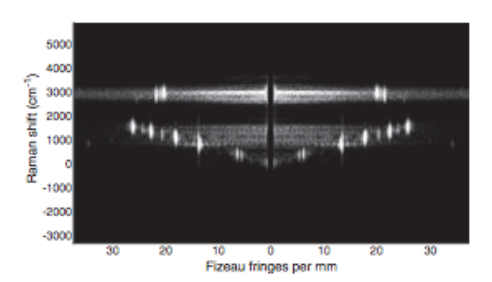


Figure 5. The above image illustrates the row by row FT of cyclohexane's xSHS Raman interferogram shown in Fig. 4. The low spatial frequencies near zero fringes per mm were masked so as to not skew the color scale by the first term in the Fourier series. Note that where a Raman feature occurs, multiplex noise is present across the entire row. This is the multiplex disadvantage (i.e., uncorrelated photon noise). By cross-dispersing spectral light before (or after) generating Fizeau fringes, the photon noise becomes correlated and the multiplex disadvantage is defeated.

Visualizing the Multiplex Disadvantage

The xSHS interferograms may be treated as N SHS interferograms, in which N equals the number of rows on the detector. As mentioned previously, multiplex noise is proportional to the square root of the total incident flux. By processing xSHS interferograms via row-by-row FT, the total incident flux becomes a function of row number and varies depending upon the summed intensities of spectral features present in that row.25 An illustration of this processing routine is depicted in Fig. 5 as a visual guide. Note that the y-axis is calibrated by wavenumber, and the x-axis is calibrated by spatial frequency. Hence, spectral features occurring in the same column are degenerated and would be sampled ambiguously by traditional SHS. However, the Amici prism induced cross-dispersion breaks this degeneracy, leading to an increase in the effective wavelength coverage beyond the Nyquist limit. The high-resolution x-axis wavelength sampling, generated by SHS, attains a spectral bin width of ~58.3 pm, and the low-resolution y-axis

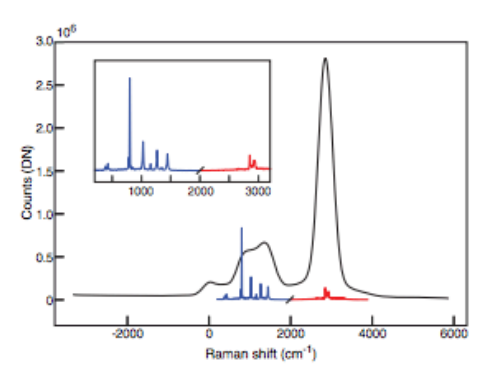


Figure 6. The xSHS and Amici prism Raman spectra of cyclohexane. Three spectra are present here: the xSHS spectrum within the Nyquist limit (blue), the xSHS spectrum beyond the Nyquist limit (red) and the Amici prism spectrum (black). A slash was placed between the blue and red xSHS spectra as a visual aid to those viewing this figure in greyscale. The Amici prism spectrum is a proxy for total incident flux in a given row of the xSHS interferogram. Note that the Raman doublet at 384.1 and 426.3 cm⁻¹ occurs at a local minimum in incident flux.

wavelength sampling, produced by the Amici prism, possesses a spectral bin width of \sim 518 pm. The dispersion provided by the Amici prism was linear within the wavelength coverage measured in these experiments (R² \sim 0.999). Multiplicative noise, known affectionately as "the grass", spans across the entirety of a row where a spectral feature occurs and can be most easily identified in the C–H stretching region for cyclohexane, occurring between 2800 and 3000 cm⁻¹, and to a lesser extent in the C–C stretch and CH₂ bending region between 801.3 and 1444.4 cm⁻¹.

Mowing the Long Grass

Most of the pixels present in Fig. 5 do not have, nor could have, Raman spectral information. The cross-dispersion provided by the Amici prism makes it so that particular spatial frequencies in the interferogram can only occur in specific columns of the row-by-row FT image. Therefore, we can create a mask to overlay Fig. 5 that maintains FT image pixels that contain spectral information while rejecting those pixels that do not. After creating and applying this mask, we can then safely integrate the remaining pixels along the x-axis that contain useful information. The results of this data reduction strategy are presented in Fig. 6. Two points are important to spell out here. First, spectral features beyond the Nyquist wavelength can be unambiguously sampled without aliasing thanks to the cross-dispersion. Second, the weak Raman modes located at 384.1 and $426.3\,\mathrm{cm}^{-1}$ are presented with high SNR because their interferograms occurred at a local minimum in terms of total incident flux. This fact will become important latter.

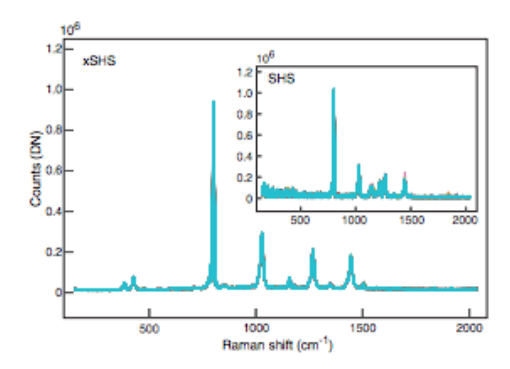


Figure 7. Plotted above are 100 spectra measured with xSHS (main figure) and 100 pseudo-SHS (sub-figure) spectra plotted, superimposed. In the pseudo-SHS spectra, the total incident flux per interferogram is much larger, which causes the low Raman shift modes at 384.1 and 426.3 cm⁻¹ to be washed out by multiplicative photon noise. In the pseudo-SHS spectra, spurious peaks appear in the CH₂ bending region caused by aliasing of the C-H stretching modes.

Beating the Multiplex Disadvantage

The purpose of xSHS is to increase the sensitivity of the instrument, relative to traditional SHS, by increasing the multiplex gain factor. In order to demonstrate this, 100 xSHS interferograms of cyclohexane were acquired and the SNR of the Raman peaks present there was calculated. To estimate SNR, we fit a Lorentzian to each peak, defined the signal as the median peak area and the noise as the median absolute deviation of those 100 peak area fits. For comparison purposes, 100 pseudo-SHS interferograms were created by summing up the columns present in the xSHS interferogram into a one-dimensional array so that the multiplex gain mimicked traditional SHS. The 100 xSHS and pseudo-SHS Raman spectra of cyclohexane are presented in Fig. 7. Clearly, the multiplex noise floor is higher in the pseudo-SHS spectra as a result of the total incident flux being higher. This point is further emphasized by the SNR calculations presented in Table I.

Earlier, we posited that SNR in FTS is proportional to the multiplex gain factor, G_{SNR} . Since the cross-dispersion provided by the Amici prism converts the total incident flux, $\overline{I(\sigma)}$, into a row-dependent parameter, xSHS interferograms can be used to verify this claim. From the row-by-row FT, the total incident flux, $\overline{I(\sigma)}$, may be approximated from the mean of the interferogram in a given row, and the intensity of a spectral feature, $I(\sigma)$, may be estimated by a spectral feature's Lorentzian peak area in a single row. The results of this processing routine are presented in Fig. 8. Since a given Raman peak occurs in multiple rows of the xSHS interferogram, this processing routine allows one to track how SNR evolves as a function of the multiplex factor gain.

Table I. SNR comparisons of Raman peaks of cyclohexane measured with xSHS and pseudo-SHS.

| Raman Shift (cm ⁻¹) | xSHS SNR | SHS SNR |
|---------------------------------|----------|-----------------|
| 384.1 | 17.2 | <i< td=""></i<> |
| 426.3 | 21 | <1 |
| 801.3 | 28.2 | 34.2 |
| 1028.3 | 31.3 | 30.6 |
| 1157.6 | 14.9 | N/A |
| 1266.4 | 25.5 | 20.7 |
| 1347.9 | 8.3 | <1 |
| 1444.4 | 26.9 | 20.5 |

Note: xSHS outperforms pseudo-SHS in terms of SNR for all but the strongest $801.3~\text{cm}^{-1}$ Raman line. For the weakest Raman features (i.e., 384.1, 426.3, and 1347.9 cm $^{-1}$), xSHS can detect these features, whereas SHS cannot.

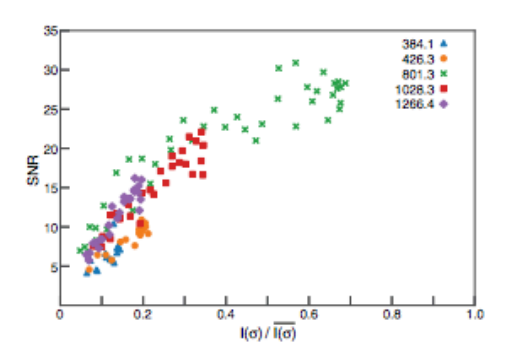


Figure 8. The SNR versus $I(\sigma)/\overline{I(\sigma)}$ scatter plot presented here illustrates how SNR attained in an SHS experiment depends upon the ratio of the peak intensity divided by the mean of the interferogram. When the signal ratio becomes significantly small enough, the SNR equals one. Below this signal ratio, a spectral feature cannot be measured.

Finally, three Raman peaks present in the xSHS spectra (i.e., 384.1, 426.3, and 1347.9 cm $^{-1}$) were claimed to have a SNR of less than one in the pseudo-SHS spectra, as stated in Table I. By defining $I(\sigma)$ as the peak area from the xSHS spectra, and $\overline{I(\sigma)}$ as the mean of the pseudo-SHS interferogram, we can now use the trends in Fig. 8 to predict what the SNR of those three peaks should be in the pseudo-SHS spectra. Those predictions are presented in Table II. Since the expected SNR is less than one, those Raman peaks in the pseudo-SHS spectra could never rise above the detection limit given their multiplex gain factors, even if an infinite number of photons were available.

The Abstemious Spatial Heterodyne Spectrometer

Spatial heterodyne spectrometers are, by nature, hungry for photons. In a typical SHS experiment, a given spectral

Table II. Predicted SNR of cyclohexane's least luminous Raman features via SHS when acquiring interferograms in the full presence of the multiplex disadvantage.

| Raman shift (cm ⁻¹) | I(σ) _{xSHS} | $I(\sigma)_{xSHS}/I(\bar{\sigma})_{SHS}$ | Expected SHS SNR |
|------------------------------------|----------------------|--|---------------------|
| 384.1 | 5.54e5 | 3.84 e-3 | 0.61 |
| 426.3 | 1.06e6 | 7.34 e-3 | 0.95 |
| 1347.9 | 3.25e5 | 2.25 e-3 | 0.98 |

feature must produce a Fizeau fringe over Nx by Ny pixels and be at least as luminous as the square root of the total incident flux. These design limitations are quite severe, especially as the density of spectral lines present increases. xSHS quells this hunger to some extent. In the ideal case, xSHS addresses these two constraints by setting $I(\sigma)$ equal to $I(\sigma)$ and limiting the production of a Fizeau fringe to just Nx pixels. In this limit, no multiplicative noise exists, so xSHS has the same noise profile as a dispersive spectrometer. If the throughputs of the two competing spectrometers were equal, the dispersive spectrometer would still maintain a sensitivity advantage by localizing the photons onto a smaller number of pixels. But the throughputs are not equal. SHS achieves 102 to 104 greater throughputs than dispersive spectrometers, depending on whether SHS is field-widened or not.

In Fellgett's era, the multiplex advantage rested upon the assumption that spare channel capacity existed in detectors that could be utilized to increase the SNR relative to quantifying the spectral elements one by one.26 Light existed, or had the potential to exist, that could not be measured in the time allotted by a scanning spectrometer. In the modern era, analogous situations can arise for remote-sensing Raman spectrometers. For example, if a Raman sample covering the entire extent of the FOV of SHS and dispersive spectrometer is scattering Raman light at uniform spectral radiant exitance, then 102 to 104 more photons would be scattered in the FOV for SHS. If the dispersive spectrometer samples the Raman feature over a few pixels, and SHS samples the same feature over a few hundred pixels, SHS could attain a sensitivity advantage, depending upon the spectral radiance of the feature, if the increased throughput offsets diluting the detection of Raman photons associated with that feature over a greater number of pixels.

Conclusion

In this work, we demonstrated that multiplicative photon noise can be suppressed by coupling SHS to an Amici prism spectrometer. The principle benefits of this method are higher fringe visibilities, broader fringe envelopes, unambiguous sampling of fringes equidistant from Littrow and beyond the Nyquist wavelength, eliminating the need for bandpass filtering, higher SNR for weak spectral features,

and low-resolution sampling of spectral features over an extensive wavelength coverage. These benefits are offset by transmission losses at the prism interfaces and additional complexity in alignment. This work is the first experimental demonstration of cross-dispersing Fizeau fringes generated by SHS via an external spectrometer for the purposes of detecting weak Raman signatures.

Declaration of Conflicting Interests

The author(s) declared no potential conflicts of interest with respect to the research, authorship, and/or publication of this article.

Funding

The author(s) disclosed receipt of the following financial support for the research, authorship, and/or publication of this article: The University of Hawaii at Manoa and The University of South Carolina (USC) would like to thank NASA (grant 80NSSC19K1024) for funding this work. USC would also like to thank the National Science Foundation (grant OCE-1829333) for funding part of this work.

ORCID iDs

Miles J. Egan (10) https://orcid.org/0000-0002-9336-4836 S. Michael Angel (10) https://orcid.org/0000-0002-1455-953X

References

- M. Lenzner, J.C. Diels. "Concerning the Spatial Heterodyne Spectrometer". Opt. Express. 2016. 24(2): 1829–1839.
- P.C.D. Hobbs. Building Electro-Optical Systems: Making It All Work. Hoboken, NJ: John Wiley and Sons, 2009. Pp. 240–242.
- P. Connes. "Spectromètre interférentiel à selection par l'amplitude de modulation". J. Phys. Radium. 1958. 19(3): 215–222.
- P. Jacquinot. "New Developments in Interference Spectroscopy". Rep. Prog. Phys. 1960. 23: 267–312.
- N.R. Gomer, C.M. Gordon, P. Lucey, S.K. Sharma, et al. "Raman Spectroscopy Using a Spatial Heterodyne Spectrometer: Proof-of-Concept". Appl. Spectrosc. 2011. 65(6): 849–857.
- N. Lamsal, S.M. Angel. "Deep-Ultraviolet Raman Measurements Using a Spatial Heterodyne Raman Spectrometer (SHRS)". Appl. Spectrosc. 2015. 69(5): 525–534.
- M.J. Egan, S.M. Angel, S.K. Sharma. "Optimizing Data Reduction Procedures in Spatial Heterodyne Raman Spectroscopy with Applications to Planetary Surface Analogs". Appl. Spectrosc. 2018. 72(6): 933–942.
- A. Zettner, A.B. Gojani, T. Schmid, I.B. Gornushkin. "Evaluation of a Spatial Heterodyne Spectrometer for Raman Spectroscopy of Minerals". Minerals. 2020. 10(2): 202.
- J.V. Sweedler, R.D. Jalkian, G.R. Sims, M.B. Denton. "Crossed Interferometric Dispersive Spectroscopy". Appl. Spectrosc. 1990. 44(1): 14–20.
- J.M. Harlander, F.L. Roesler, J.G. Cardon, C.R. Englert, R.R. Conway. "SHIMMER: A Spatial Heterodyne Spectrometer for Remote Sensing of Earth's Middle Atmosphere". Appl. Opt. 2002. 41(7): 1343–1352.
- A.I. Sheinis, E. Mierkiewicz, F. Roesler, J. Harlander, A. Bodkin. "A Spatial Heterodyne Spectrometer for Diffuse H-α Spectroscopy". Proc. SPIE. 2008. 7014: 701401-1–701401-12.
- B.B. Behr, A.R. Hajian, A.T. Cenko, M. Murison, et al. "Stellar Astrophysics with a Dispersed Fourier Transform Spectrograph I.

- Instrument Description and Orbits of Single-Lined Spectroscopic Binaries". Astrophys. J. 2009. 705: 543-553.
- 13. A.R. Hajian, B.B. Behr, A.T. Cenko, R.P. Olling, et al. "Initial Results from the UNSO Dispersed Fourier Transform Spectrograph". Astrophys. J. 2007. 661: 616-633.
- 14. D.J. Erskine, J. Edelstein, E. Wishnow, M. Sirk, et al. "High-Resolution Broadband Spectroscopy Using Externally Dispersed Interferometry at the Hale Telescope: Part 2, Photon Noise Theory". J. Astron. Telesc. Instrum. Sys. 2016. 2(4): 1-22.
- 15. A.G. Kim, E.V. Linder, J. Edelstein, D. Erskine. "Giving Cosmic Redshift Drift a Whirl". Astropart. Phys. 2015. 62: 195-205.
- 16. P.K. Morgan, J.R. Scott, I. Jovanovic. "Hybrid Interferometric/ Dispersive Atomic Spectroscopy of Laser-Induced Uranium Plasma". Spectrochim. Acta, Part B. 2016. 116: 58-62.
- 17. D. Riebe, T. Beitz, C. Dosche, H.G. Löhmannsröben, et al. "High-Resolution Spectrometer Using Combined Dispersive and Interferometric Wavelength Separation for Raman and Laser-Induced Breakdown Spectroscopy (LIBS)". Appl. Spectrosc. 2014. 68(9): 1030-1038.
- 18. J.M. Harlander. Spatial heterodyne Spectroscopy: Interferometric Performance at Any Wavelength Without Scanning. [Doctoral

- Dissertation.] Madison, Wisconsin: University of Wisconsin-Madison, 1991.
- 19. F.D. Kahn. "The Signal: Noise Ratio of a Suggested Spectral Analyzer". 1959. Astrophys. J. 129: 518–520. 20. T. Hirschfeld. "Fellgett's Advantage in UV–Vis Multiplex
- Spectroscopy". Appl. Spectrosc. 1976. 30(1): 68-69.
- 21. P. Luc, S. Gerstenkorn. "Fourier Transform Spectroscopy in the Visible and Ultraviolet Range". Appl. Opt. 1978. 17(9): 1327-1331.
- 22. S. Gerstenkorn, P. Luc. "Emission Spectra Studies by Means of Fourier Transform Spectroscopy in the Visible Range". Nouv. Rev. Optique. 1976. 7(3): 149-157.
- 23. N.J. Everall, J. Howard. "Signal-to-Noise Considerations in FT-Raman Spectroscopy". Appl. Spectrosc. 1989. 43(5): 778-781.
- 24. J. Zhao, R.L. McCreery. "Multichannel FT-Raman Spectroscopy: Noise Analysis and Performance Assessment". Appl. Spectrosc. 1997. 51(11): 1687-1697.
- 25. P.D.Barnett, K.A.Strange, S.M.Angel. "Improving Spectral Results Using Rowby-Row Fourier Transform of Spatial Heterodyne Raman Spectrometer Interferogram". Appl. Spectrosc. 2017.71(6): 1380-1386.
- 26. P. Fellgett. "Conclusions on Multiplex Methods". J. Physique Colloques. 21967. 8(C2): 165-171.